Model for Gas Damping in Air Gaps of RF MEMS Resonators

T. Veijola, A. Lehtovuori

DTIP 2007 of MEMS & MOEMS Stresa, Italy, 25-27 April 2007

MODEL FOR GAS DAMPING IN AIR GAPS OF RF MEMS RESONATORS

Timo Veijola and Anu Lehtovuori

Helsinki University of Technology, Department of Electrical and Communications Engineering
P.O.Box 3000, FIN-02015 HUT, Finland, timo.veijola@tkk.fi, Tel: +358-9-4512293, Fax: +358-9-4514818.

Abstract

Damping in air gaps is studied at RF frequencies and modelled with a viscoelastic wave propagation model, since the traditional squeezed-film damping model is not valid in the MHz regime. The FEM study shows that above a certain frequency the wave propagation in the air gap can be modelled assuming closed damper borders. This closed-border problem is solved analytically from the linearized Navier-Stokes equations in 1D. This results in a compact model for the mechanical impedance that includes the damping, inertial, and spring forces. The model produces the gas resonances in the air gap when the wavelength of the acoustic wave is smaller than the gap dimensions. The model is applicable in cases where the frequency of oscillation in a squeezed-film damper is so high that the gas is trapped in the gap. The model is applied in calculating damping due to air in a RF MEMS disk resonator.

1. INTRODUCTION

Capacitively coupled MEMS resonators are characterized by very small gap sizes, well below 1 μm [1]–[3]. To achieve high Q values, RF MEMS resonators are normally operated at very low pressure to minimize the damping due to gas flow in the air gaps. This is not always necessary, since the squeezed-film damping effect that dominates the damping behaviour at low frequencies may be negligible at high frequencies [3].

Damping in air gaps of oscillating structures has been traditionally modelled with the Reynolds equation [4], [5]. It considers the viscous gas flow and compressibility. The Reynolds equation is usable only up to a certain frequency where the inertial forces can be neglected (Reynolds number $\ll 1$). This limitation can be avoided considering the inertia in the gap flow [6]. This leads to a 2D viscoelastic wave propagation model. Beltman has applied it in modelling problems where the pressure across the small gap can be assumed constant [7], [8].

When the length of the acoustic wave is comparable to the height of the gap, the problem becomes more complicated. The pressure is no more constant across the gap and the density is not proportional to the pressure. Moreover, neither isothermal nor adiabatic assumptions can be made, the temperature variation and thermal conductivity must be accounted for in the model. This leads to another damping mechanism in addition to the viscous damping and a 3D wave propagation model is needed for an accurate analysis. FEM tools are required in solving such model equations [9], [10].

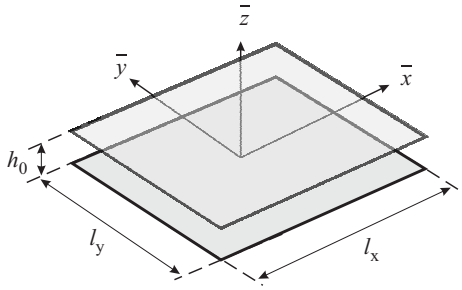

Figure 1: A squeeze-film damper consisting of parallel surfaces moving perpendicularly.

In this paper, the linearized Navier-Stokes (N-S) equations are first presented and the 1D viscoelastic wave propagation equations are derived. Its variables are the pressure, density, velocity and temperature, that all vary across the gap. The equations are solved analytically considering the boundary conditions. Due to the small dimensions in micromechanical devices, slip conditions are used for temperature [11].

2D FEM simulations are used to verify the resulting mechanical impedance model and to show how open-border and closed-border models give exactly the same results above a certain frequency. This verifies that the gas is trapped in the gap at high frequencies and the acoustic wave propagates only in the direction across the gap. The problem reduces to 1D and the wave propagation model can be solved analytically.

The model is applied in calculating the gas damping in an air gap of a RF MEMS disk resonator [1]–[3].

ISBN: 978-2-35500-000-3

2. VISCOELASTIC WAVE PROPAGATION MODEL

In this chapter, a wave propagation model is derived for the structure shown in Fig. 1. The figure shows the dimension of the damper surface (l_x, l_y) and the air gap h_0. Normalized coordinates (x, y, and z) are used in the text instead of the absolute coordinates ($\overline{x}$, $\overline{y}$, and $\overline{x}$) shown in the figure. The upper surface moves and acts on the gas in the air gap. The damper is characterized by mechanical impedance. It is the force F acting on the surface divided by its velocity w_0.

$$Z_\mathrm{m} = -\frac{F}{w_0} \tag{1}$$

2.1. Characteristic Numbers

The behaviour of the flow in a narrow air gap is described in the frequency domain by a few characteristic numbers. The Reynolds number $\mathtt{Re}$ (the square of the shear wave number s) is the ratio between inertial and viscous forces:

$$s^2 = \mathtt{Re} = \frac{\omega h_0^2 \rho_0}{\eta}, \tag{2}$$

where ρ_0 is the density of the gas, η is the viscosity coefficient, and h_0 is the characteristic height of the air gap.

The reduced frequency $k = \omega h_0/c_0$ is scaled with nominal displacement h_0 and the speed of sound $c_0 = \sqrt{\gamma P_\mathrm{A}/\rho_0}$, where γ is the specific heat ratio and P_A is the ambient pressure.

The Knudsen number $\mathtt{Kn} = \lambda/h_0$ is a measure of gas rarefaction and λ is the mean free path. The Prandtl number $\mathtt{Pr}$ characterizes the thermal properties. Here, the square root of $\mathtt{Pr}$ is used,

$$\phi = \sqrt{\mathtt{Pr}} = \sqrt{\frac{\eta C_\mathrm{p}}{\kappa}}, \tag{3}$$

where C_p is the specific heat at constant pressure and κ is the thermal conductivity.

K_T is the "thermal Knudsen number" [11] that characterizes the temperature jump at the surfaces due to rarefied gas

$$K_\mathrm{T} = \frac{2-\alpha_\mathrm{T}}{\alpha_\mathrm{T}} \left[\frac{2\gamma}{\gamma+1}\right] \frac{K_\mathrm{n}}{\phi^2}, \tag{4}$$

where α_T is the energy accommodation coefficient.

2.2. Linearized Navier-Stokes Equations

The dimensionless notation by Beltman [7] is used here for the linearized time-harmonic Navier-Stokes equations:

$$\begin{aligned} \mathrm{i}u &= -\frac{g}{k\gamma}\frac{\partial p}{\partial x} + \frac{1}{s^2}\left[g^2\frac{\partial^2 u}{\partial x^2} + \left(\frac{g}{a}\right)^2\frac{\partial^2 u}{\partial y^2} + \frac{\partial^2 u}{\partial z^2}\right] \\ &\quad + \frac{1}{3}\frac{g}{s^2}\frac{\partial}{\partial x}\left[g\frac{\partial u}{\partial x} + \left(\frac{g}{a}\right)\frac{\partial v}{\partial y} + \frac{\partial w}{\partial z}\right] \end{aligned} \tag{5}$$

$$\begin{aligned} \mathrm{i}v &= -\frac{g}{ak\gamma}\frac{\partial p}{\partial y} + \frac{1}{s^2}\left[g^2\frac{\partial^2 v}{\partial x^2} + \left(\frac{g}{a}\right)^2\frac{\partial^2 v}{\partial y^2} + \frac{\partial^2 v}{\partial z^2}\right] \\ &\quad + \frac{1}{3}\frac{g}{as^2}\frac{\partial}{\partial y}\left[g\frac{\partial u}{\partial x} + \left(\frac{g}{a}\right)\frac{\partial v}{\partial y} + \frac{\partial w}{\partial z}\right] \end{aligned} \tag{6}$$

$$\begin{aligned} \mathrm{i}w &= -\frac{1}{k\gamma}\frac{\partial p}{\partial z} + \frac{1}{s^2}\left[g^2\frac{\partial^2 w}{\partial x^2} + \left(\frac{g}{a}\right)^2\frac{\partial^2 w}{\partial y^2} + \frac{\partial^2 w}{\partial z^2}\right] \\ &\quad + \frac{1}{3}\frac{1}{s^2}\frac{\partial}{\partial z}\left[g\frac{\partial u}{\partial x} + \left(\frac{g}{a}\right)\frac{\partial v}{\partial y} + \frac{\partial w}{\partial z}\right] \end{aligned} \tag{7}$$

$$g\frac{\partial u}{\partial x} + \frac{g}{a}\frac{\partial v}{\partial y} + \frac{\partial w}{\partial z} = -\mathrm{i}k\rho \tag{8}$$

$$p = \rho + T \tag{9}$$

$$\mathrm{i}T = \frac{1}{s^2\phi^2}\left[g^2\frac{\partial^2 T}{\partial x^2} + \left(\frac{g}{a}\right)^2\frac{\partial^2 T}{\partial y^2} + \frac{\partial^2 T}{\partial z^2}\right] + \mathrm{i}\frac{\gamma-1}{\gamma}p, \tag{10}$$

where u, v, and w are velocity components in the x-, y-, and z-direction, respectively. The equations are in normalized form such that velocities u, v, and w are normalized to the speed of sound c_0 and the dimensions x, y, and z are normalized with the characteristic dimensions l_x, l_y, and h_0, respectively. p, ρ, and T represent small relative variations around P_A, ρ_0 and T_A, respectively. The narrowness of the gap $g = h_0/l_\mathrm{x}$ and ratio of the plate $a = l_\mathrm{y}/l_\mathrm{x}$ as shown in Fig. 1.

2.3. 1D Wave Propagation Model

In his "narrow gap" solution (Appendix B in [7]), Beltman simplifies equations assuming $g/s \ll 1$ and negligible z-directional velocity w compared with the velocities u and v. Here the situation is different: small gap is not assumed, but velocities u and v are assumed to be negligible. This reflects the trapped gas situation. Now, it yields

$$\mathrm{i}w = -\frac{1}{k\gamma}\frac{\partial p}{\partial z} + \frac{4}{3s^2}\frac{\partial^2 w}{\partial z^2} \tag{11}$$

$$\frac{\partial w}{\partial z} = -\mathrm{i}k\rho \tag{12}$$

$$p = \rho + T \tag{13}$$

$$\mathrm{i}T = \frac{1}{s^2\phi^2}\frac{\partial^2 T}{\partial z^2} + \mathrm{i}\frac{\gamma-1}{\gamma}p. \tag{14}$$

Instead of zero boundary conditions, slip boundary conditions for temperature T [11] are applied:

$$T|_{z=1} = -K_\mathrm{T}\left.\frac{\partial T}{\partial z}\right|_{z=1}, \quad T|_{z=0} = K_\mathrm{T}\left.\frac{\partial T}{\partial z}\right|_{z=0}. \tag{15}$$

ISBN: 978-2-35500-000-3

2.4. Simple Solution

First, the approximate case is studied for a simple model. Since the model is derived for relatively high frequencies, large s is assumed in Eq. (14). Temperature becomes

$$T = \frac{\gamma - 1}{\gamma} p, \tag{16}$$

and density from Eq. (13) results in $\rho = p/\gamma$. This condition is equivalent with the adiabatic assumption (The isothermal assumption, that is good at low frequencies only, would result in $\rho = p$). The pressure is solved from Eq. (12) resulting in

$$p = -\frac{\gamma}{\mathrm{i}k} \frac{\partial w}{\partial z}. \tag{17}$$

Equation (11) describes the relation between pressure and velocity in the z-direction and after inserting Eq. (17) into it,

$$\mathrm{i}w = \left(\frac{1}{\mathrm{i}k^2} + \frac{4}{3s^2} \right) \frac{\partial^2 w}{\partial z^2} \tag{18}$$

results. The velocity function

$$w(z) = \frac{w_0 \sinh(qz)}{\sinh(q)}, \tag{19}$$

where

$$q = -\mathrm{i} \left(\frac{1}{k^2} + \mathrm{i} \frac{4}{3s^2} \right)^{-\frac{1}{2}} \tag{20}$$

is a solution of Eq. (18) and satisfies the boundary conditions $w(1) = w_0$ and $w(0) = 0$. At low frequencies, $q \to 0$ and $w(z)$ approaches to linear velocity $w_0 z$ corresponding the approximation by Beltmann.

The pressure is now from Eq. (17)

$$p(1) = -\frac{\gamma}{\mathrm{i}k} \left. \frac{\partial w}{\partial z} \right|_{z=1} = -\frac{\gamma}{\mathrm{i}k} \frac{w_0 q}{\tanh(q)}, \tag{21}$$

resulting to an unnormalized force of $F = l_\mathrm{x} l_\mathrm{y} P_\mathrm{A} p(1)$.

2.5. Resonant Frequencies

The expression for resonant frequencies can be approximated from Eq. (21) assuming a large s compares to k (small viscosity), then q is simplified to $-\mathrm{i}k$. The resonance occur when the denominator in (21) is zero or infinity. This happens when $\mathrm{i}q = N\pi/2$, where $N = 1, 2, 3, \ldots$. Odd values of N give antiresonances, while even values of N give resonances. The approximate Nth resonant frequency is

$$f_N = \frac{N}{4h_0} \sqrt{\frac{\gamma P_\mathrm{A}}{\rho_0}} = \frac{N c_0}{4h_0} \tag{22}$$

The first antiresonance f_1 especially is interesting, since if the device is operated close to this frequency, a very small damping due to gas can be achieved. For air at atmospheric pressure, $f_1 = 87.7\,\mathrm{MHz}$ for a gap of $1\mu\mathrm{m}$.

2.6. Exact Solution

The exact solution for Eqs. (11) – (14) is presented in the Appendix. The boundary conditions for velocity are $w(0) = 0$ and $w(1) = w_0$, and the temperature has slip conditions at the surfaces. The solution gives velocity w, pressure p, temperature T and density ρ in the gas as function of z. The calculation of these variables requires the evaluation a lot of complex auxiliary variables.

The result is presented as an unnormalized mechanical impedance that is calculated from the pressure acting on the upper surface.

$$Z_\mathrm{m} = -\frac{l_\mathrm{x} l_\mathrm{y} P_\mathrm{A} p(1)}{w_0}. \tag{23}$$

3. MODEL VERIFICATION

FEM simulations were performed with a solver for dissipative acoustic flow [10] included in Elmer [9] software. It solves the linearized N-S equations (5) – (10).

Here, a 1D damper geometry is assumed, that is, the y-dimension of the damper is assumed to be much larger than the x-dimension. This assumption does not limit the usability of the model, since the final model does depend only on the surface area, not on the shape of the damper. In the simulations, the damper length is assumed to be $l_\mathrm{x} = 20\,\mu\mathrm{m}$ and the air gap height is $h_0 = 1\,\mu\mathrm{m}$ ($l_\mathrm{y} = 1\,\mathrm{m}$).

Table 1: Gas parameters used in the simulations.

	Description	Value	Unit
P_A	pressure	101	$10^3\,\mathrm{N/m^2}$
T_A	temperature	300	$^o\mathrm{K}$
η	viscosity coefficient	18.5	$10^{-6}\,\mathrm{N\,s/m^2}$
ρ_0	density of air	1.155	$\mathrm{kg/m^3}$
C_P	specific heat	1.01	$10^3\,\mathrm{J/kg/K}$
γ	specific heat ratio	1.4	
κ	heat conductivity	0.025	$\mathrm{W/m/K}$
λ	mean free path	68	$10^{-9}\,\mathrm{m}$
α_T	energy accomm.	1	

A sinusoidal velocity amplitude of $0.1\,\mathrm{m/s}$ was used as the excitation. The symmetry of the structure was utilized in the FEM simulations; only a half of the air gap was simulated. Boundary conditions $p(\pm l_\mathrm{x}/2) = 0$

ISBN: 978-2-35500-000-3

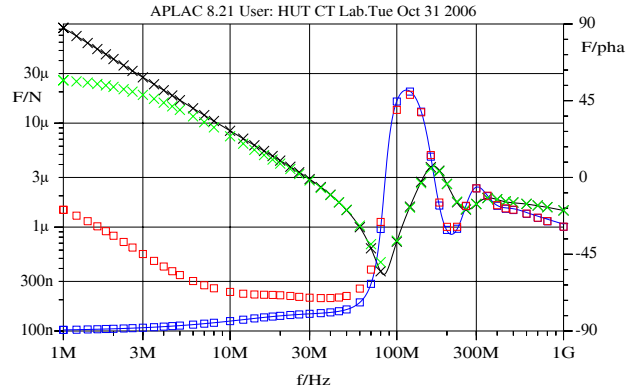

Figure 2: Exact solution in the case of closed ends (——) compared with the FEM simulation results of open and closed ends cases (magnitudes × and phases □).

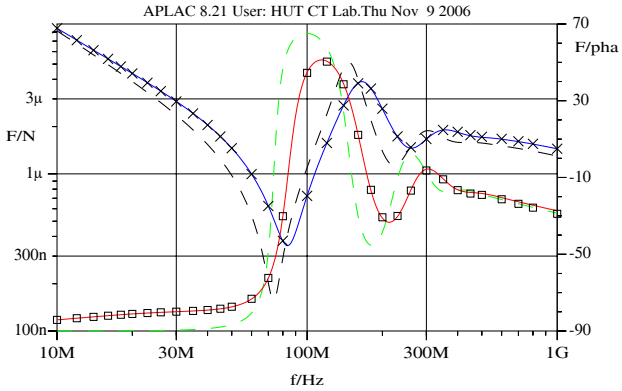

Figure 3: Exact solution (——) compared with simple solution (– – –) and results of FEM simulation (magnitudes × and phases □).

were used at the damper borders. Slip boundary conditions for temperature were used and ideally thermal conducting surfaces were assumed. A mesh of 8000 elements was used, and the simulation was performed at 49 frequencies from 1 MHz to 1 GHz. The gas parameters are shown in Table 1.

3.1. Open/closed Damper Boundaries

The justification to the use of closed borders instead of the open ones when the gas is trapped, is studied. Fig. 2 shows FEM simulations of the same damper with closed and open borders. The amplitude and phase responses are identical above 70 MHz. This is close to the first resonant frequency at 88 MHz.

3.2. Comparison Between the Simple and the Exact Model

Fig. 3 shows the difference between simple and exact solutions. The response of the exact model is identical with FEM simulation results. The resonant frequency of the simple solution matches well with the one calculated from Eq. (22). The difference between the simple and exact models is considerable.

3.3. Damping Coefficient and Spring Constant

Fig. 4 presents the damping coefficient and the spring constant given by the model. The damping coefficient $c = \mathrm{Re}(Z_\mathrm{m})$ has a minimum at the first resonance. When this minimum is matched with the resonance of the mechanical structure, the damping due to gas is very low and the quality factor of the resonator is limited, in practice, by other loss mechanisms.

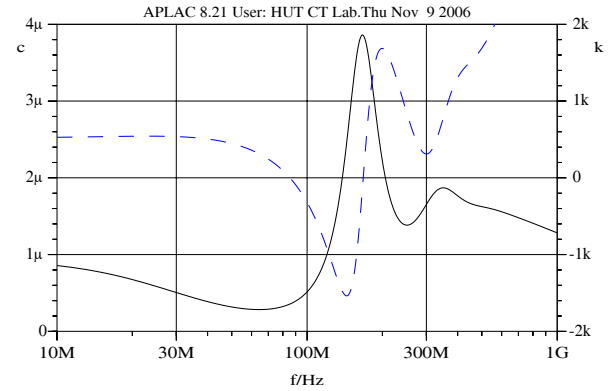

Figure 4: Damping coefficient c (——) in Kg/s and the spring constant k (– – –) in N/m as a function of frequency.

The spring constant $k = \mathrm{Im}(Z_\mathrm{m})\omega$ is constant at small frequencies but crosses the zero at the first resonance. A negative spring constant indicates inertial force, not a spring force. The spring-like behaviour takes over at higher frequencies.

4. AIR DAMPING IN A DISK RESONATOR

The model is applied here in predicting damping in the air gap of a disk resonator documented in [3]. Figure 5 shows the structure of the resonator. Table 2 shows dimensions for two resonators. Radial oscillation of the disk is assumed. The air gap is very small compared to the radius of the resonator thus the parallel-plate

ISBN: 978-2-35500-000-3

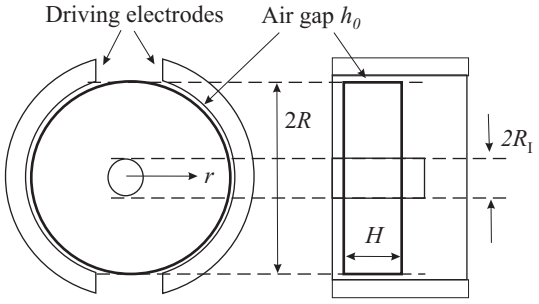

Figure 5: Structure of a disk resonator forming a RF filter.

model can be applied. l_x is here the width of the air gap H, while l_y is the length of the gap $2\pi R$.

Table 2: Parameters for disk resonators.

	Description	Disk 1	Disk 2	Unit
R	disk radius	18	10	μm
H	disk height	2.1	2.1	μm
h_0	air gap	0.087	0.068	μm
f_r	resonant freq.	151.3	274	MHz
c	damping coeff.	19	14	10^{-9} kg/s

Table 2 indicates the damping coefficients c given by the model. According to the quality factor measurements [3] in vacuum and at ambient air pressure, the damping coefficients estimated here explain only about a fourth part of the total damping due to air.

5. CONCLUSIONS

Design aids for estimating damping in air gaps of RF MEMS resonators were presented in the form of compact models. With these models, the Reynolds equation has been extended to be applicable to rapidly oscillating surfaces and rare gas conditions. The model is in agreement with FEM simulation results.

FEM simulations show that the model can be used in predicting the damping and spring forces due to gas accurately at frequencies that are larger than the first resonant frequency. This validated the assumption for trapped gas and closed damper borders in the analysis. Slip conditions are used to have an accurate model also for small air gaps.

It was shown that the model is useful in predicting the resonances due to gas. The resonator can be designed such that the minimum of the damping coefficient matches the resonance of the device.

The comparison shows that for an accurate model it is necessary to include the full temperature dependency in the model. However, the simple model gives a rough estimate of the behaviour of the damping and spring forces.

The damping coefficients estimated here for disk resonators could not explain the total damping due to air. There are probably other damping mechanisms that act on the disk surfaces.

REFERENCES

[1] B. Bircumshaw *et al.*, "The Radial Bulk Annular Resonator: Towards a 50 Ω RF MEMS Filter," *Proceedings of Transducers'03*, (Boston, MA), pp. 875–878, 2003.

[2] J. R. Clark, W.-T. Hsu, and C. T.-C. Nguyen, "High-Q VHF Micromechanical Contour-Mode Disk Resonators," *Technical Digest IEEE Int. Electron Devices Meeting*, pp. 493–496, 2000.

[3] P. Y. Wang and E. Y. Yu, "Nearly Free-Molecular Channel Flow at Finite Pressure Ratio," *The Physics of Fluids*, vol. 15, no. 6, pp. 1004–1009, 1971.

[4] J. J. Blech, "On Isothermal Squeeze Films," *Journal of Lubrication Technology*, vol. 105, pp. 615–620, October 1983.

[5] W. S. Griffin, H. H. Richardson, and S. Yamanami, "A Study of Fluid Squeeze-Film Damping," *Journal of Basic Engineering, Trans. ASME*, vol. 88, pp. 451–456, June 1966.

[6] T. Veijola, "Compact Models for Squeezed-Film Dampers with Inertial and Rarefied Gas Effects," *Journal of Micromechanics and Microengineering*, vol. 14, pp. 1109–1118, 2004.

[7] W. M. Beltman, P. J. van der Hoogt, R. M. E. J. Spiering, and H. Tijdeman, "Air Loads on a Rigid Plate Oscillating Normal to Fixed Surface," *Journal of Sound and Vibration*, vol. 206, pp. 217–241, 1997.

[8] W. M. Beltman, "Viscothermal Wave Propagation Including Acousto-Elastic Interaction, Part I: Theory," *Journal of Sound and Vibration*, vol. 227, pp. 555–586, 1999.

[9] Elmer, "Elmer – Finite Element Solver for Multiphysical Problems," 2006. http://www.csc.fi/elmer.

[10] M. Malinen *et al. Proc. of the 4th European Congress on Computational Methods in Applied Sciences and Engineering* (P. Neittaanmäki *et al.*, eds.), (Jyväskylä, Finland), July 2004.

[11] G. E. Karniadakis and A. Beskok, *Micro Flows, Fundamentals and Simulation.* Springer, Heidelberg, 2002.

ISBN: 978-2-35500-000-3

APPENDIX

An exact solution for Eqs. (11) – (14) is presented considering the boundary conditions. After some manipulation, the following fourth order differential equation results

$$\frac{1}{s^2\phi^2}\left(\frac{1}{\mathrm{i}k}+\frac{4k\gamma}{3s^2}\right)w''''-\left(\frac{\mathrm{i}4k}{3s^2}+\frac{\mathrm{i}k\gamma}{s^2\phi^2}+\frac{1}{k}\right)w''-kw=0 \tag{24}$$

for velocity $w(z)$ and

$$\frac{1}{s^2\phi^2}\left(\frac{1}{\mathrm{i}k}+\frac{4k\gamma}{3s^2}\right)T''''-\left(\frac{\mathrm{i}4k}{3s^2}+\frac{\mathrm{i}k\gamma}{s^2\phi^2}+\frac{1}{k}\right)T''-kT=0 \tag{25}$$

to temperature $T(z)$ as well. In this appendix, the derivatives with the respect to z are denoted with primes ($T'''' = \partial^4 T/\partial z^4$).

This homogenous linear equation with constant complex coefficients has characteristic equation

$$\alpha_1 r^4+\alpha_2 r^2-k=0, \tag{26}$$

$$\alpha_1 = \frac{1}{s^2\phi^2}\left(\frac{1}{\mathrm{i}k}+\frac{4k\gamma}{3s^2}\right) \tag{27}$$

$$\alpha_2 = -\left(\frac{\mathrm{i}4k}{3s^2}+\frac{\mathrm{i}k\gamma}{s^2\phi^2}+\frac{1}{k}\right) \tag{28}$$

The roots of Eq. (26) are

$$r_1 = \sqrt{\frac{-\alpha_2+\sqrt{\alpha_2^2+4\alpha_1 k}}{2\alpha_1}},\ r_3=-r_1 \tag{29}$$

$$r_2 = \sqrt{\frac{-\alpha_2-\sqrt{\alpha_2^2+4\alpha_1 k}}{2\alpha_1}},\ r_4=-r_2 \tag{30}$$

and then the solution of Eq. (24) is

$$w(z)=C_1e^{r_1 z}+C_2e^{r_2 z}+C_3e^{r_3 z}+C_4e^{r_4 z}. \tag{31}$$

Constants C_1, C_2, C_3, and C_4 are determined with boundary conditions. For velocity, $w(0)=0$ and $w(1)=w_0$ and two missing boundary conditions are to temperature: $T(1)=-K_\mathrm{T}T'(1)$, $T(0)=K_\mathrm{T}T'(0)$. Therefore, the temperature is written as function of velocity w. Eqs. (11) – (14) reduce now to

$$T' = A_1 w + A_2 w'' \tag{32}$$

$$w' = A_3 T + A_4 T'', \tag{33}$$

where

$$A_1 = -\mathrm{i}k\gamma, \tag{34}$$

$$A_2 = \left(\frac{1}{\mathrm{i}k}+\frac{4k\gamma}{3s^2}\right), \tag{35}$$

$$A_3 = -\frac{\mathrm{i}k}{\gamma-1}, \tag{36}$$

$$A_4 = \frac{k\gamma}{(\gamma-1)s^2\phi^2}. \tag{37}$$

Solving T from Eqs. (32) and (33) and p from Eqs. (12), (13) and (38) yields

$$T(z)=B_1w'+B_2w''', \tag{38}$$

$$p(z)=-\frac{1}{\mathrm{i}k}w'+T=\left(B_1-\frac{1}{\mathrm{i}k}\right)w'+B_2w''', \tag{39}$$

where B_1 and B_2 are the auxiliary variables:

$$B_1=\frac{1-A_1A_4}{A_3},\ B_2=-\frac{A_2A_4}{A_3}. \tag{40}$$

Equation (38) can be used to utilize boundary conditions for temperature to solve the velocity:

$$T(1) = B_1w'(1)+B_2w'''(1)=0, \tag{41}$$

$$T(0) = B_1w'(0)+B_2w'''(0)=0. \tag{42}$$

After applying $w(0)=0$ and $w(1)=w_0$ in addition to the conditions above, the following system of equations results:

$$C_1+C_2+C_3+C_4=0, \tag{43}$$

$$C_1e^{r_1}+C_2e^{r_2}+C_3e^{r_3}+C_4e^{r_4}=w_0, \tag{44}$$

$$C_1Q_1+C_2Q_2+C_3Q_3+C_4Q_4=0, \tag{45}$$

$$C_1Q_1e^{r_1}+C_2Q_2e^{r_2}+C_3Q_3e^{r_3}+C_4Q_4e^{r_4}=0, \tag{46}$$

where $Q_i=B_1r_i+B_2r_i^3$. The coefficients C_i in Eq. (31) are

$$C_1 = \frac{H_2P_3M-GP_3-MP_2}{P_1+P_2L-H_1P_3-H_2P_3L}, \tag{47}$$

$$C_2 = LC_1+M, \tag{48}$$

$$C_3 = G-H_1C_1-H_2C_2, \tag{49}$$

$$C_4 = -C_1-C_2-C_3, \tag{50}$$

where

$$G=w_0/(e^{r_3}-e^{r_4}), \tag{51}$$

$$H_1=(e^{r_1}-e^{r_4})/(e^{r_3}-e^{r_4}), \tag{52}$$

$$H_2=(e^{r_2}-e^{r_4})/(e^{r_3}-e^{r_4}), \tag{53}$$

$$L=\frac{H_1K_3-K_1}{K_2-H_2K_3}, \tag{54}$$

$$M=\frac{-GK_3}{K_2-H_2K_3}, \tag{55}$$

$$K_i=B_1(r_i-r_4)+B_2(r_i^3-r_4^3), \tag{56}$$

and

$$P_i=B_1(r_ie^{r_i}-r_4e^{r_4})+B_2(r_i^3e^{r_i}-r_4^3e^{r_4}). \tag{57}$$

Now the values for variables $p(z)$, $w(z)$, $T(z)$ can be calculated from Eqs. (39), (31) and (38), respectively. The density is simply $\rho(z)=p(z)-T(z)$.

ISBN: 978-2-35500-000-3